A comparative study on the efficacy of dual-pol and full-pol ASAR data in radiative transfer modeling for forest above-ground biomass estimation

Faseela V. Sainuddin, Sanid Chirakkal, Smitha V. Asok & Deepak Putrevu

Published online: 29 Jan 2024.

Submit your article to this journal ↗

View related articles ↗

View Crossmark data ↗

Taylor & Francis
Taylor & Francis Group

Check for updates

A comparative study on the efficacy of dual-pol and full-pol ASAR data in radiative transfer modeling for forest above-ground biomass estimation

Faseela V. Sainuddin [a], Sanid Chirakkal [b], Smitha V. Asok [a]
and Deepak Putrevu [b]

aDepartment of Environmental Sciences, All Saints' College, Thiruvananthapuram, India; bAdvanced Techniques Development Division (ATDD), Space Applications Centre, ISRO, Ahmedabad, India

ABSTRACT

In this study, a comprehensive evaluation of the potential of dual-polarization and full-polarization L- and S-band airborne SAR (LS-ASAR) data (ISRO's dual-frequency airborne SAR mounted on NASA's Gulfstream III aircraft) in forest above-ground biomass (AGB) estimation has been carried out. The study area comprises the temperate forests of the Lenoir landing site in Southwest Alabama, United States of America. A trunk scattering model based on Vector Radiative Transfer (VRT) theory is used in this study to estimate the AGB. Full-polarization ASAR data inversion retrieves three critical biophysical parameters: tree height, diameter at breast height (DBH), and tree count, whereas with dual-polarization ASAR data, the model is limited to retrieving only two parameters (tree height and DBH). These parameters are then employed in a suitable allometric equation to estimate the AGB over the study area. Validation of the retrieval results is performed through comparison with ground-truth measurements taken from the study site. The findings demonstrate that the inversion of L-band full-polarized data yields the highest correlation ($R^2 = 0.87$, RMSE = 20.37 t/ha), revealing high accuracy in AGB estimation. The L-band dual-polarized data shows a high correlation ($R^2 = 0.83$, RMSE = 30.66 t/ha), indicating reasonable accuracy. However, the S-band data, both full and dual-polarized, reveals weaker correlations with higher RMSE values ($R^2 = 0.59$, RMSE = 55.07 t/ha, and $R^2 = 0.49$, RMSE = 58.31 t/ha, respectively), suggesting a lower degree of reliability. This study emphasizes the pre-eminence of L-band fully polarized data inversion for reliable and accurate AGB estimation while also showing the utility of relatively ubiquitous dual-pol data (L-band) to achieve reasonable accuracy for the same.

1. Introduction

Forests significantly contribute to combating climate change by acting as natural carbon storage systems in the global carbon balance (Van der Werf et al. 2009). Understanding carbon stocks and fluxes is vital for assessing the carbon cycle's current state and its

CONTACT Faseela V. Sainuddin ✉ faseelahzain@gmail.com ▣ Department of Environmental Sciences, All Saints' College, Thiruvananthapuram 695007

response to climate change (Martin, Thomas, and Chave 2011). To understand the link between forest biomass and its carbon content, it's vital to have detailed insights into forest biomass, taking into account its regional variations and changes over time (Martin, Thomas, and Chave 2011).

However, the spatial variability of forest carbon stocks and fluxes remains poorly quantified (Quegan et al. 2019). Hence, calculating forest biomass seeks to minimize ambiguities in global carbon dynamics and deepen our knowledge of carbon reservoirs and emissions from forests (Le Toan et al. 2011). The growing availability of SAR data has facilitated research across a wide range of fields (Modava, Akbarizadeh, and Soroosh 2018, 2019; Periasamy 2018), which has in turn led to the development of different methods, notably in the estimation of above-ground biomass in forests.

The estimation of above-ground biomass (AGB) using synthetic aperture radar (SAR) backscatter has been extensively investigated in a variety of forest habitats, from tropical to boreal (Bouvet et al. 2018; Santoro and Cartus 2018; Tanase et al. 2014). Airborne and satellite SAR sensors have been employed to gauge forest characteristics across different radar frequency bands, including p-, L-, S-, C-, and X-bands (Mitchard et al. 2014; Saatchi et al. 2011). The radar sensitivity to forest structure varies with wavelength (or frequency), polarizations, and incidence angles, all of which have impacts on the penetration capability of microwave radiation into the canopy and the backscattering from canopy elements (Du, Ulaby, and Dobson 2000; Saatchi and McDonald 1997). Additionally, the type of canopy (from intact to open, homogeneous to complex structure) and environmental factors like moisture content affect the sensitivity of radar signals to forest structure (Lucas et al. 2010). The sensitivity of radar backscatter to AGB varies across different polarizations and frequencies. This is evident across multiple frequency bands. For instance, in the P-band with a wavelength of 30–100 cm (Saatchi et al. 2011; Sandberg et al. 2011; Santos et al. 2003), the L-band spanning 15–30 cm (Cartus, Santoro, and Kellndorfer 2012; Lucas et al. 2010), the S-band covering 7.5–15 cm (Ningthoujam et al. 2016, 2017), and the C-band ranging from 4–8 cm (Dobson et al. 1995; Pulliainen, Kurvonen, and Hallikainen 1999). In general, these studies have revealed that long wavelengths, like the L- and P-bands, are more sensitive to AGB than the S- and C-band data (Luckman, Baker, and Wegmueller 2000; Naidoo et al. 2015; Saatchi et al. 2011). This can be attributed to the rapid attenuation of shorter wavelengths as they traverse the forest canopy and interact with the woody components. In contrast, longer wavelengths experience less attenuation, enabling the backscatter signal to capture and correlate with information from the woody elements, thus establishing a stronger relationship with AGB. Previous studies revealed that the backscatter from high-frequency bands seems to saturate at lower levels of above-ground biomass ranging between 20 and 50 t/ha (Castro, Sanchez-Azofeifa, and Rivard 2003; Imhoff 1995; Luckman, Baker, and Wegmueller 2000), the L-band backscatter has a sensitivity on AGB ranging from 75 to 150 t/ha (Cartus, Santoro, and Kellndorfer 2012; Neumann et al. 2012; Robinson et al. 2013), and with the P-band, it can reach up to 300 t/ha (Hoekman and Quiriones 2000; Le Toan et al. 2011; Saatchi et al. 2011, 2007; Sandberg et al. 2011). Most studies on the estimation of forest above-ground biomass employing synthetic aperture radar were focused on using L-band data due to the lack of P-band space-borne SAR data and the studies consistently highlight the high temporal consistency and greater sensitivity of L-band SAR in capturing forest biophysical attributes, surpassing the abilities of shorter

wavelength SAR (Askne et al. 2003; Baker and Luckman 1999; Sandberg et al. 2011; Santoro et al. 2006, 2009). Furthermore, studies have indicated that among the SAR backscatter intensities, cross-polarization demonstrates the highest sensitivity in estimating above-ground biomass (Balzter et al. 2002; Castel et al. 2001; Dobson et al. 1992; Ranson and Sun 1994).

Estimating forest AGB from SAR backscatter involves employing a diverse range of approaches. In the research conducted by Santoro and Cartus (Santoro and Car the methods were grouped into three main categories: empirical regression approaches, non-parametric approaches, and semi-empirical or physically-based approaches. Empirical regression models (Dobson et al. 1995; Harrell et al. 1997), like linear and multiple linear models, are commonly used to link AGB with SAR backscatter observations, with improved accuracy achieved through cross-polarized data. However, it is crucial to consider potential deviations from the assumed linear relationship, leading to under- or over estimation, particularly in certain AGB ranges. Non-parametric models (Breidenbach, Næsset, and Gobakken 2012; Jung et al. 2013; McRoberts, Gobakken, and Næsset 2012; Mitchard et al. 2013; Mutanga, Adam, and Cho 2012; Saatchi et al. 2009) utilize computational algorithms to learn from observations, constructing and refining multiple models until convergence is achieved. Their advantage, especially when incorporating multiple input and auxiliary datasets, becomes more prominent. However, optimal performance often requires a substantial amount of training data, which may be limited or unavailable, particularly for large-scale mapping purposes. This study focuses on the utilization of the physical model to describe forest backscattered intensity by considering the underlying scattering mechanisms within the forest (Antropov et al. 2013; Cartus et al. 2011; Cartus, Santoro, and Kellndorfer 2012; Kurvonen, Pulliainen, and Hallikainen 1999; Sainuddin et al. 2021, 2023; Santoro et al. 2011). In contrast to empirical models, these models provide increased reproducibility due to their reduced dependency on field data (Houborg, Soegaard, and Boegh 2007; Quan, He, and Li 2015; Yebra et al. 2013). These models, having limited components, represent the overall forest backscatter based on forest structural attributes and their interactions with microwaves. This modeling approach computes the total backscatter by summing the contributions from both the forest canopy and the forest floor. Significantly, in forest regions, the L-band backscatter predominantly originates from the volume scattering of the forest canopy and from the ground scattering where there are gaps in the canopy (Chauhan, Lang, and Ranson 1991; Karam et al. 1995; Pulliainen, Kurvonen, and Hallikainen 1999; Skriver, Mortensen, and Gudmandsen 1994; Way et al. 1994). Even though the L-band wave can penetrate dense tropical forests, the impact of interactions between the trunk and ground on the overall backscatter is typically seen as restricted. This is attributed to reasons like diffuse scattering on the uneven forest ground and signal attenuation within the canopy layer (Dobson et al. 1992; Pulliainen, Kurvonen, and Hallikainen 1999). The comparison of full polarimetric data with dual-polarized data for estimating above-ground biomass in forested areas is relatively under explored, with only a limited number of existing studies available. For instance, Tanase et al (Tanase et al. 2014). conducted a study that evaluated parametric and non-parametric models using dual and full polarization systems to

estimate AGB in semi-arid forests. In a different study, Pereira et al (Pereira et al. 2018). investigated the relative efficacy of full-pol SAR data in contrast to single- and dual-pol SAR data for AGB estimation in the Amazonian wetlands. Sandberg et al (Sandberg et al. 2011). conducted another study where they investigated the estimation of above-ground biomass in a hemiboreal forest and compared the results obtained from regression models using single and multi-polarizations of the L- and p- bands.

In recent years, there has been a notable emphasis among space organizations on developing radar sensors specifically designed for observing AGB and forest structures from space. One such mission is the NISAR (NASA ISRO SAR) mission, a collaborative effort between the US National Aeronautic and Space Administration (NASA) and the Indian Space Research Organization (ISRO). The mission aims to launch a SAR satellite that provides globally available dual-polarized (HH and HV) L-band (and S-band in certain regions) data, offering sensitivity to forest AGB (NISAR 2020). It operates on a 12-day repeat pass and uses single-look-complex (SLC) data to obtain a higher spatial resolution of less than 10 m. Another project, the BIOMASS mission from the European Space Agency (ESA), is set to launch in 2024. This mission will employ a space-borne P-band SAR for the first time to retrieve forest height and AGB estimates, providing global coverage of tropical forests and partial coverage of boreal forests (European Space Agency 2008; Le Toan et al. 2011). These missions, along with other space-borne SAR sensors like the German Aerospace Center's TanDEM-L which is scheduled to launch in 2024, the Japanese Advanced Land Observing Satellite-2 Phased Array L-band SAR-2 (ALOS-2 PALSAR-2), and the Argentinean SAtélite Argentino de Observación COn Microondas (SAOCOM), contribute to the improved monitoring of global forests.

Currently, there exists a research gap in the systematic evaluation of the dual and full polarization modes of SAR data, implemented in the context of radiative transfer (RT) modeling, for estimating above-ground biomass. This research explores the efficacy of LS-ASAR backscatter, in both dual and full polarization modes, in assessing the above-ground biomass in temperate forest areas. Importantly, the LS-ASAR mission, acting as a precursor to the NISAR mission, offers valuable insights into the potential of NISAR data for accurate AGB estimation. The approach leverages a physical scattering model that combines a vegetation layer RT model based on the framework proposed by Karam and Fung (Karam and Fung 1988) with the improved integral equation model (I^{2}EM) introduced by Fung and Chen (Fung and Chen 2010) to represent the backscattering from the underlying surface. By integrating these two models, the total backscatter intensity is simulated. In this proposed methodology, the vegetation is represented as a layer devoid of foliage, resembling a group of dielectric cylinders of specific heights. This modeling strategy allows for the extraction of backscattering data from above-ground woody structures, which are presumed to comprise the majority of the tree's biomass. For the estimation of biophysical parameters that are pertinent to AGB, a strategy that involves the constrained nonlinear optimization of a cost function was used. In the case of dual-pol L- and S-bands, the model allows for the retrieval of tree height and trunk radius. For fully polarized L- and S-bands, the methodology enables the retrieval of an additional parameter – tree count – alongside tree height and trunk radius. Finally, the retrieved biophysical parameters are applied to an allometric equation to estimate the AGB for the entire scene. The key novelties of this study include:

- Systematic evaluation of the dual and full polarization modes of Synthetic Aperture Radar data, particularly in the context of radiative transfer modeling, with the aim of estimating above-ground biomass.
- An in-depth examination of the utility of LS-ASAR backscatter for estimating above-ground biomass and a definitive conclusion as to the performance of one band over the other.
- A categorical conclusion with regard to dual-pol versus full-pol S- and L-band SAR data in AGB modeling, which is likely to extrapolate in the case of P-band data as well.

The paper is structured as follows: Section 2 outlines the specific study area and details the data used for the research. The methodology section (section 3) details the theory of simulating backscatter intensities with the scattering model, retrieving biophysical parameters, and estimating above-ground biomass for selected SAR frequencies. Section 4 presents the findings of this study, focusing on the application of LS-ASAR backscatter in both dual and full polarization modes for biomass estimation. This section offers a comprehensive analysis, comparing the results of this work with established research in the domain and evaluating the potential of the given frequencies, in dual or full polarization, for accurate forest AGB estimation. The study concludes with final observations and implications in Section 5.

2. Study area and data

2.1. Study area

The study area, known as the Lenoir landing site, holds special significance as it has been meticulously chosen as one of the prime areas of interest for the NISAR mission. The region is situated in the southwestern part of Alabama, near the Tombigbee River, and falls within the boundaries of the Choctaw National Wildlife Refuge (Figure 1). The study site stretches over 706 km^2 and its center is located at $31^056'$N and $88^09'$W with elevation ranges of 9 to 138 m above MSL. The region has an average annual precipitation of about 1385 mm and an average annual temperature of 18.1^0C. Due to the vicinity of the Tombigbee River, which is prone to spring floods, several sites in the region are at risk of flooding. The area features woody wetlands, deciduous hardwood trees, and meadows. The area's vegetation is primarily characterized by a pine-oak mixed forest with a dense canopy, where pines are typically found in elevated areas with relatively lower water levels, while oaks are dispersed throughout the entire region, even within the marshy wetlands. The common tree species include loblolly pine (*Pinus taeda*), shagbark hickory (*Carya ovata*), black gum (*Nyssa sylvatica*), green ash (*Fraxinus pennsylvanica*), sweetgum (*Liquidambar styraciflua*), mockernut hickory (*Carya alba*), possumhaw (*Ilex decidua*), and the oaks. The ground cover is also made up of a variety of cypress (*Taxodium spp*.), poison ivy (*Toxicodendrom radicans*), bamboo, grass, and smilax.

2.2. Forest Inventory and analysis

The field survey was conducted at the Lenoir landing area in conjunction with the LS-ASAR validation experiment. The study relied on field survey data conducted by the national
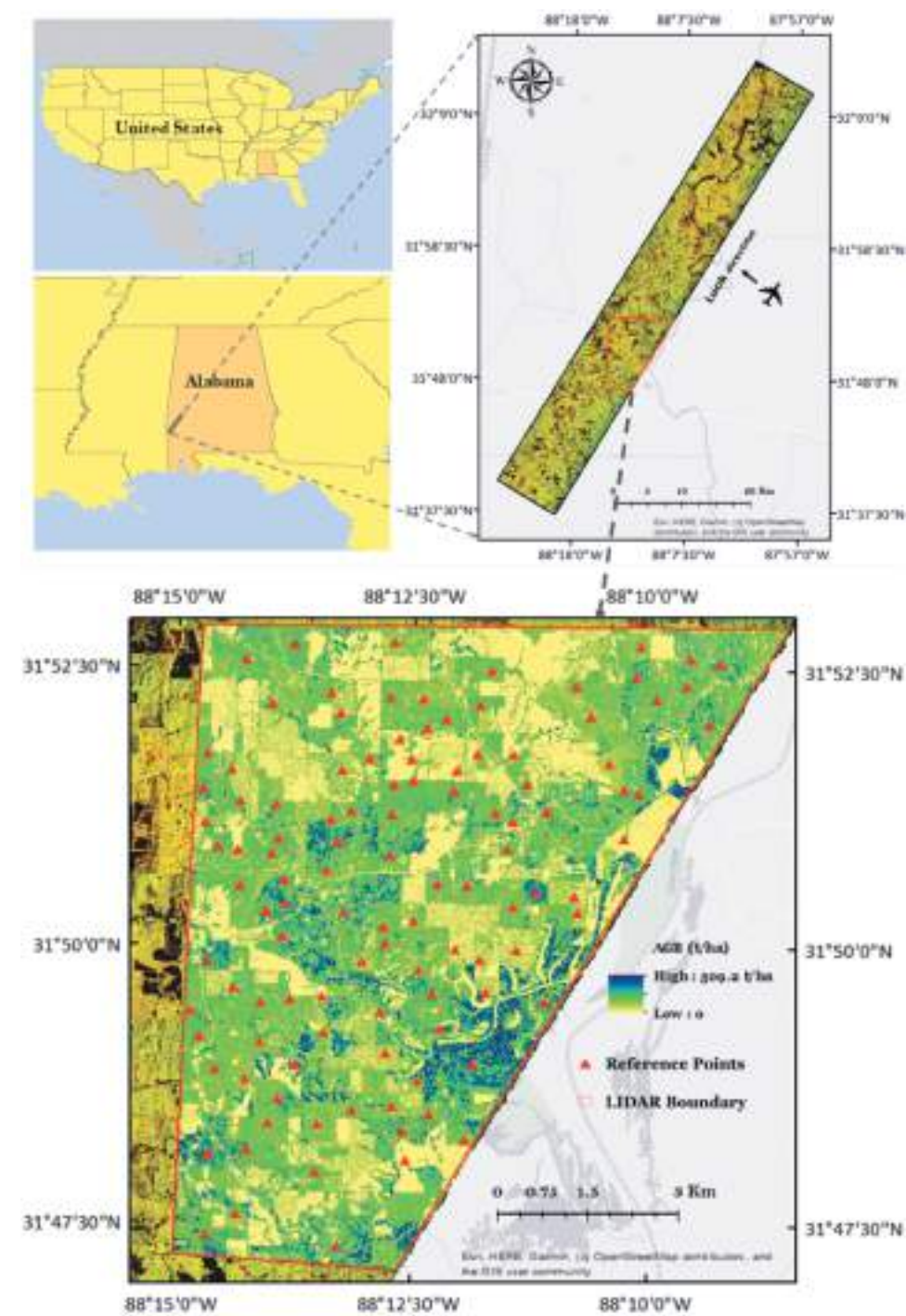
Figure 1. Upper left: geographic location of the study area. Upper right: FCC image comprising of HH (R), HV (G), and VV (B) intensities of L-band ASAR data over the study area, and the red rectangle shows the boundary of the LIDAR data. Lower center: LIDAR AGB map and reference points.
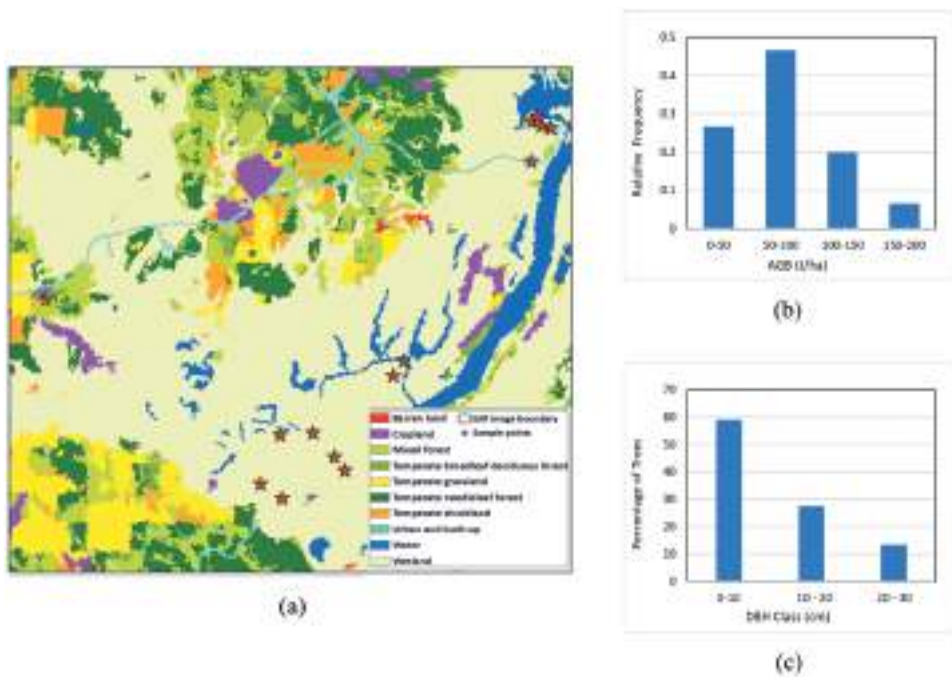
Figure 2. a) landcover map by NLCD with field sample location points for the study site b) frequency distribution of field-measured above-ground biomass c) distribution of trees in DBH classes.

ecological observatory network (NEON) (NEON 2020) from October to December 2021. Fourteen sample plots, each spanning 40 m × 40 m, were chosen within the SAR observation zone for evaluation (Figure 2(a)). The collected ground truth information on biophysical parameters includes tree count, tree height, DBH, and tree species names. The predominant vegetation classes in the study area were determined using the national land cover database (NLCD) from the multi-resolution land characteristics consortium (MRLC) (MRLC 2022). Although the study area encompasses multiple vegetation classes, the wetlands were the sole category with a substantial quantity of data points, allowing for model building. A dual-band GPS device was employed to precisely determine the coordinates of the plot boundaries. The DBH of all trees exceeding 2.5 cm in diameter within the plot was measured. The tree height was measured for all trees in the plot. The ranges of the mean tree height (HT) and mean DBH were 7.22 to 15.95 m and 9.12 to 21.72 cm, respectively. Forest parameter statistics based on the survey conducted in the study area are presented in Table 1. The study used the allometric equation proposed by Stovall et al (Stovall et al. 2018), which is presented in Equation (1).

Table 1. Summary statistics for field sample data in the study area.

Variables	AGB (t/ha)	MDBH (cm)	MHT (m)	Tree Count (trees/ha)
Minimum	32.76	9.12	7.22	137.5
Maximum	156.77	21.72	15.95	575
Mean	76.41	16.79	11.03	237.98
SD	38.09	3.95	2.71	113.95

$$\text{Biomass} = exp(\beta_0 + \beta_1 \ln(\text{DBH}^2 * \text{HT})) \tag{1}$$

Where $\beta_0 = -2.75$, and $\beta_1 = 0.919$. Figure 2(b,c) display the frequency distribution of AGB based on field measurements, as well as the distribution of trees across DBH classes, respectively. The total AGB for each plot fluctuates between 32.76 t/ha and 156.77 t/ha, with an average value of 76.41 t/ha.

AGB = above ground biomass, MDBH = mean diameter at breast height, MHT = mean height, SD = standard deviation.

2.3. AGB reference map

A map delineating reference above-ground biomass is derived from canopy heights measured using small-footprint LIDAR technology, aiming to reduce potential discrepancies encountered when directly correlating SAR-AGB relationships with confined plot areas. The canopy height data, constructed at a 1 m resolution, was derived using data from the NEON Airborne Observation Platform's Optech LIDAR Gemini instrument (NEON 2020). A power function-based regression, optimized through least-squares minimization, is applied to correlate plot-level AGB with the LIDAR-measured canopy height (Saatchi et al. 2011). This method results in a reference AGB map with a spatial resolution of 1 m. In LIDAR AGB map, 110 polygons, each measuring (40 m × 40 m) and randomly distributed (Figure 1), are selected along with the twelve field-measured sample points to validate the predicted AGB maps.

2.4. Airborne SAR data

This study used L- and S-band airborne SAR (LS-ASAR) amplitude data acquired at the Lenoir landing site on 10th July 2021. Geo-coded level-2 products were downloaded from NASA JPL (JPL 2022). LS-ASAR L- and S-band images were radiometrically calibrated using the Equation (2).

$$\sigma^0(dB) = 10log10(DN^2 - N) + 10log10(\sin(i_p)) - K_{dB} \tag{2}$$

where $\sigma^0(dB)$ is the backscattering coefficient, DN is the digital number, N is the image noise bias, i_p is the per-pixel incidence angle, and K_{dB} is the calibration constant. LS-ASAR is a precursor airborne mission to the space-borne dual-frequency L and S-Band NASA ISRO synthetic aperture radar (NISAR) mission, where the L-band is provided by NASA and the S-band is ISRO's contribution. As part of their preparation, NASA and ISRO are sourcing and analyzing L- and S-band SAR images using ISRO's ASAR device. This instrument has been attached to NASA's Gulfstream III plane, employing the antenna pod and navigation equipment from NASA's Uninhabited Aerial Vehicle Synthetic Aperture Radar (UAVSAR) radar setup. After the completion of Phase 1 in December 2019, the subsequent Phases 2 and 3 of the ASAR initiative were conducted in June and July 2021. This involved revisiting data from Alaska and the Western U.S. and gathering fresh data from New Orleans and the Eastern Coast. The system is engineered to function at a height of 8 km and move at a speed of 120 m/s. The center frequencies are 3.2 GHz for S-band and 1.25 GHz for

Table 2. Characteristics of LS-ASAR data.

Characteristics	Descriptions
Frequency (GHz)	L-band: 1.25 & S-band: 3.2
Polarizations	full-Pol (HH, HV, VH, VV)
Product type	L2-GEOREF
Look direction	left
Pixel spacing	2 m × 2 m
Near incidence angle (degrees)	26
Far incidence angle (degrees)	53
Acquisition date	July 10, 2021
Acquisition type	stripmap

L-band. The system design for LS-ASAR is based on the system specifications of NISAR. More details on the airborne SAR imagery used for the study are given in Table 2.

3. Methodology

The radiative transfer model employed in this study was utilized for the simulation of SAR backscatter with the objective of estimating biophysical variables related to above-ground biomass, thereby enabling AGB estimation. The retrieval of biophysical parameters was executed through the distinct processing of dual- and full-polarized ASAR data in the L- and S-bands. Python scripts were developed for forward modeling as well as inverse modeling. These scripts were designed to handle both full-polarization and dual-polarization (with simplifying assumptions) data sets. For quantitative analysis of the retrieval accuracy, the outcomes were evaluated by comparing them to ground truth data. The methodology is structured around three major steps.

(1) Simulating backscatter intensities from the vegetation canopy using the integrated RT & I^{2}EM models
(2) Estimating the biophysical parameters from the simulated backscatter intensity by the application of constrained non-linear optimization of a cost function
(3) Estimation of above-ground biomass for the entire scene of L-band (Full and dual-pol) and S-band (Full and dual-pol).

Figure 3 illustrates the comprehensive methodology framework.

3.1. Simulation of Backscatter Intensities

The dielectric cylinder model adopted in this study was originally introduced in (Karam and Fung 1988). In the model, the vegetation stands were segmented into two distinct layers: a layer comprising dielectric finite-length cylinders representing defoliated trunks, and the underlying rough ground layer. The total backscatter intensity (σ^0) of a pixel is the sum of contributions from both the trunk layer and the ground layer below. The simulation focused solely on the defoliated trunks and did not consider saplings, lianas, or under-story vegetation. The backscattering coefficient for the layer containing circular cylinders placed over a rough floor was determined using the first-order solution of the
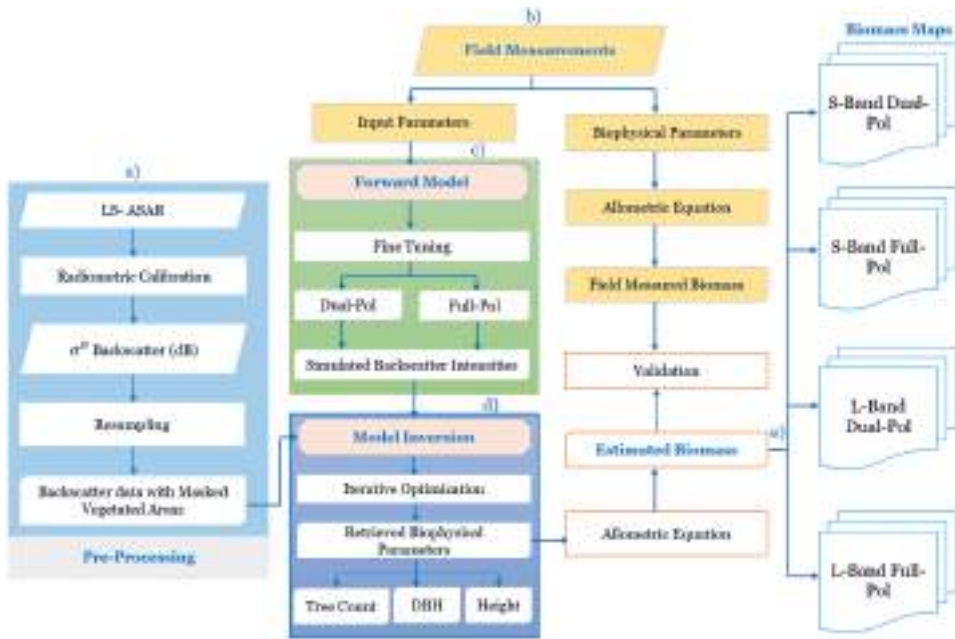
Figure 3. Schematic work-flow for retrieval of above-ground biomass from the integrated microwave scattering model.

radiative transfer equation. The expression for the total backscattering coefficient, denoted as σ^0_{total}, is given by:

$$\sigma^0_{total} = \sigma^0_{trunk} + \sigma^0_{ground} \tag{3}$$

where σ^0_{trunk} represents the backscattering coefficient of the trunk layer and σ^0_{ground} represents the backscattering coefficient of the ground layer. For simulating the backscattering coefficients (full-pol being HH/HV/VV and dual-pol being HH/HV) at the L- and S-bands, alterations were applied to the initial backscatter framework suggested by Karam and Fung (Karam and Fung 1988). The backscattering coefficient, denoted as σ^0_{trunk}, for the layer of cylinders that signifies the trunk, is illustrated by the subsequent formula:

$$
\begin{aligned}
\sigma^0_{trunk} = & \left[4\pi \cos \Theta_i / <K_e^p(i)> + <K_e^q(i)>\right] \} \\
& \cdot \{1 - exp\left[-\left(<K_e^p(i)> + <K_e^q(i)>\right)n_0 dsec\Theta_i\right]\} \\
& \cdot <|f_{pq}(i,i)|^2>
\end{aligned}
\tag{4}
$$

In the above equation, n_0 stands for the tree count density of cylinders for each unit of volume, and d denotes the thickness of the layer populated by vegetation. The incidence angle is represented by Θ_i. The term $<|f_{pq}(-i,i)|^2>$ refers to the measure of the scattering amplitude and $<K_e^p(i)>$ represents the extinction coefficient within the cylinder layer.

The complexity and stochastic nature of the medium are interpreted by analyzing the orientation of the trunks using probability density functions. It is presumed that the layer of cylindrical scatterers exhibits uniform orientation in the azimuthal direction. In the absence of correlation between the orientation angles of the

cylinders, the succeeding Equation (5) can be employed to estimate the joint probability distribution function:

$$p(\alpha, \beta, \gamma) = p(\alpha)p(\beta)p(\gamma) \tag{5}$$

In the equation, the angles mentioned are recognized as the Tait-Bryan angles. Due to the symmetric property of cylinders, these can be appropriately defined by applying Euler angles.

$$\gamma = 0 \quad \text{and} \quad p(\gamma) = 1 \tag{6}$$

For more details of the cylinder model, refer to these previous studies (Karam and Fung 1982, 1988; Sainuddin et al. 2021, 2023; Wait 1955, 1959). The scattering model developed by Karam and Fung Karam and Fung (1988) employs the Kirchhoff model in the scalar domain to calculate soil backscatter. This technique characterizes the scattering properties of a rough soil surface, assuming the soil to be a smooth, gently undulating dielectric continuum. However, this assumption has proven inadequate for modeling radar scattering across a wide range of soil moisture and surface roughness. To offer a more robust simulation of soil surface scattering, the study adopts an advanced model known as the improved integral equation model (I^{2}EM), initially proposed by Fung and Chen (Fung and Chen 2010). The I^{2}EM model for surface backscatter is remarkably adaptable and applicable to numerous soil surface situations. The general equation, expressed in Equation 7, enables the computation of the backscattering coefficient from the surface layer utilizing the I^{2}EM model.

$$\sigma_{\text{ground}}^0 = \frac{k^2}{4\pi} exp[-4k_z^2\sigma^2]\{\left|(2k_z\sigma)f_{pp} + \frac{\sigma}{4}(F_{pp1} + F_{pp2})\right|^2 w(2k\sin\Theta, 0)$$
$$+ \sum_{n=2}^{\infty} \left|(2k_z\sigma)^n f_{pp} + \frac{\sigma}{4}F_{pp1}(2k_z\sigma)^{n-1}\right|^2 \frac{w^n(2k\sin\Theta0, 0)}{n!}\} \tag{7}$$

In this equation, the symbols $p = v, h$ represent different polarizations, with k being the radar wave number. The term σ is used to denote the RMS height, and Θ symbolizes the incidence angle. The terms f_{vv} and f_{hh} be represented by the following equations: $f_{vv} = 2R_v/\cos\Theta$ and $f_{hh} = -2R_h/\cos\Theta$, where R_v and R_h stand for Fresnel reflection coefficients associated with vertically and horizontally polarized waves, respectively. The factors w and w^n correspond to the surface spectra of the two-dimensional Fourier transforms of the correlation coefficient and its nth power, respectively. For a comprehensive understanding of the equation, refer to the work of Fung and Chen (Fung and Chen 2010).

In order to simulate the backscatter intensities, the integrated RT & I^{2}EM models utilize a specific set of input parameters, including SAR frequency, incident angle, polarization, soil moisture, surface RMS height, correlation length, vegetation dielectric constant, tree height, tree count density, and trunk radius. While some variables, such as tree count density or tree height, can be directly measured, others, like correlation length or RMS height, pose significant challenges in their measurement. In such cases, estimated values or values obtained from relevant literature were utilized. In this study, Figure 4 provides, in block-diagram format, the list of canopy, surface, and
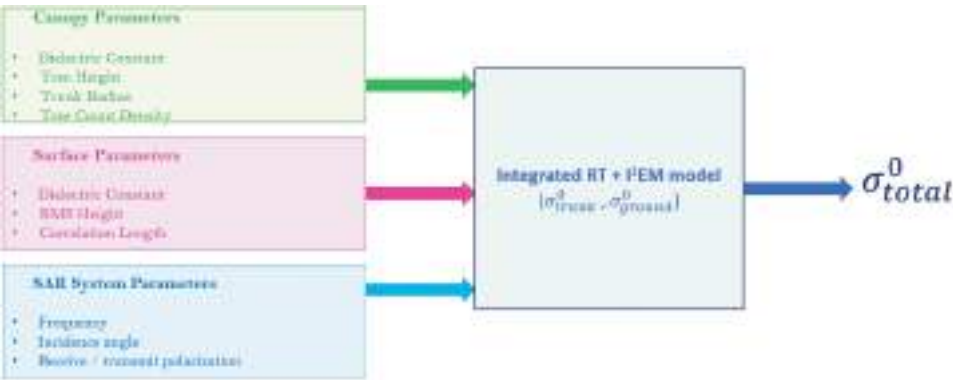
Figure 4. Block-diagram representation of the canopy, surface, and SAR system parameters for the integrated microwave scattering model.

Table 3. Input parameters for scattering models.

Layer	Parameter	Values
Surface Layer	Correlation length (m)	0.08
	RMS Height (m)	1.3
	Dielectric Constant	11.12–1.12j
Canopy Layer	Dielectric Constant (dual & full-pol)	9.37+3.15j
	Tree Count Density (m^{-3}) (dual-pol)	0.025

SAR system parameters required to specify the model to simulate the total back-scattering coefficient (σ^0_{total}) from the vegetated terrain. Table 3 shows the parameters required as input for the scattering models. The dielectric constant for the surface layer was estimated using Topp's equation (Topp, Davis, and Annan 1980) based on data from the average soil moisture content obtained from the Soil Moisture Active Passive (SMAP) satellite. The RMS height was sourced from the documentation available for the Lenoir landing site (NEON 2020). In the context of SAR applications, the sensitivity of SAR signals to variations in soil surface RMS height is recognized as a critical factor influencing surface scattering. This understanding is supported by several key studies in the field (Bryant et al. 2007; Dubois, Van Zyl, and Engman 1995; Oh, Sarabandi, and Ulaby 1992; Shi et al. 1997), which collectively highlight the reduced impact of spatial correlation due to SAR azimuthal processing and multi-looking. Based on this literature consensus, an approximate value for the correlation length was adopted. The tree count density per unit volume (n0) and the vegetation dielectric constant were fixed in the case of dual-polarization SAR data inversion, while for full-polarization SAR data inversion, only the vegetation dielectric constant was fixed. A detailed description of this procedure is available in the following subsection.

3.2. Inversion of simulated backscatter intensities

The process of retrieving biophysical parameters from the backscatter coefficients simu-lated from the integrated scattering model constitutes the inversion problem in this context. To unravel this problem, the study employed a unique hybrid Iterative

Optimization (IO) strategy that combines Genetic Algorithms (GA) (Goldberg 1989) and a gradient-based minimization method, leveraging the strengths of both evolutionary and conventional optimization techniques. This method is founded on the principle of optimizing a merit function, specifically the difference between the observed and the model-simulated backscatter coefficients. If **Y** represents the vector of backscatter coefficients, its relationship with the model **M** and the vector of input parameters can be mathematically represented as:

$$\mathbf{Y} = \mathbf{M}(\Theta, \mathbf{X}) + \epsilon \tag{8}$$

In this context, Θ represents the array of model input parameters. Throughout the inversion procedure, a value function S(X) is minimized for n data points to derive X, which are the optimized values of tree biophysical characteristics.

$$S(X) = \sum_{i=1}^{n} [Y_i - M(\Theta, X_i)]^2 \tag{9}$$

The nonlinear evaluation function can be tackled through the integration of evolutionary and conventional optimization algorithms. A starting point for the parameters is necessary, and they are repeatedly refined until the value function is close to its minimum values. It is relevant to understand that the optimization problem is non-linear, bound by constraints, and deals with a scalar function of multiple variables. To manage these characteristics, the hybrid strategy first employs the GA for a global search over the parameter space. The parameter bounds for height, trunk radius, and tree count density per unit volume (n_0) are strictly defined, ranging from 3 to 25 m, 0.03 to 0.5 m, and 0.0001 m^{-3} to 0.05 m^{-3} respectively. To offer clarity and match conventional metrics, the trunk radius and tree count density per unit volume are then converted to diameter at breast height (DBH) and tree count (total number of trees per hectare), respectively. Post-GA, the solution is further refined using the gradient-based Limited-memory Broyden-Fletcher-Goldfarb-Shanno (L-BFGS-B) algorithm (Morales 2002). This technique ensures that the optimal parameter values, which minimize the merit function, fall within the predefined parameter ranges. This combination of GA and L-BFGS-B forms a robust hybrid optimization framework that can efficiently solve the non-linear, constrained nature of the problem, providing a reliable solution.

The inversion procedure for dual polarization data necessitated the fixation of two parameters of the forward model, specifically the tree count density per unit volume (n_0) and the dielectric constant associated with vegetation. This was achieved through the use of two ground-measured sample points (which are then not used in subsequent validation of AGB and other parameters). For the full-pol data inversion, only the vegetation dielectric constant was held constant. For the corresponding date, soil moisture data was obtained from the Soil Moisture Active Passive (SMAP) satellite. Other key parameters, including the surface RMS height, were obtained from existing literature, while an approximate value was utilized for the correlation length. Consequently, by fixing these parameters based on ground-measured data available, the complexity of the model was significantly reduced, allowing for a more streamlined and focused analysis in both dual and full-polarization modes to simulate the corresponding backscatter intensities. A distinct set of twelve data points was set aside for independent validation of the model-derived parameters and the AGB. The biophysical

values estimated from the model inversion were then plugged into the allometric Equation 1 to calculate the above-ground biomass. The trunk radius retrieved from the inversion process is transformed into the more commonly used metric of DBH, which is utilized as a key parameter for estimating above-ground biomass. For the full-pol scenario, the model generated predictions for the n_0 of each pixel, in addition to tree height and DBH. Using these predicted n_0 values, the total count of the trees in each plot was subsequently estimated and then incorporated with the corresponding AGB values of each pixel in order to facilitate the estimation of the total AGB per pixel. On the contrary, for dual-pol data, the model inversion resulted in the retrieval of only the tree height and DBH, while n_0 was kept constant. In this case, the AGB was estimated using the allometric equation based on the retrieved tree height and DBH. The estimated AGB per pixel was further multiplied with an optimal value, representing the total number of trees per plot set specifically for distinct vegetation types, to determine the total AGB for each pixel. To evaluate the accuracy of the retrieval process, three statistical metrics were employed: the coefficient of determination (R^2), the root mean square error (RMSE), and the mean absolute error (MAE). Finally, spatial maps of AGB were generated for both dual and full polarization scenarios of the LS-ASAR data. To streamline the computation process during optimization, the SAR images were multi-looked into 30 m × 30 m pixel sizes. As a final step in the procedure, areas that were devoid of vegetation were masked, ensuring they were exempted from the computation. This comprehensive and systematic strategy aids in assessing the efficacy of both dual and full polarization data at two distinct frequencies in the estimation of AGB and related biophysical attributes from the integrated scattering model.

4. Results

This section explores the findings of the study regarding the utilization of LS-ASAR backscatter in dual and full polarizations for estimating above-ground biomass in the study area. The investigation provides valuable insights into the performance and potential of multi-frequency, multi-polarization SAR data in accurately estimating forest AGB.

4.1. General performance of Model inversion

In this subsection, the focus is on assessing the performance of the inverse modeling employing the LS-ASAR backscatter (in dual and full polarizations) for retrieving forest biophysical parameters. Radiative transfer models, including the dielectric cylinder scatter model proposed by Karam and Fung (Karam and Fung 1988) and I²EM surface scatter model proposed by Fung and Chen (Fung and Chen 2010), underwent modifications to integrate first-order scatter mechanisms from both the ground and trunk layers. For the full-pol data inversion, HH/HV/VV combinations were used, while for the dual-pol data inversion, HH/HV combinations were used. The parameters retrieved from the inversion of the model were plotted against the parameters measured in the field. This research made use of 14 sample plots. Out of these, two points were utilized to constrain and set the parameters of the forward model, while the remaining twelve points were kept separate and used as independent validation data.

4.1.1. *Performance of Model inversion with dual-pol data*

This section presents the performance of the model inversion using dual-pol data (HH and HV) in S- and L-frequencies. In the forward modeling of the dual-pol case, two parameters of the model were fixed: tree count density and vegetation dielectric constant, utilizing two ground-measured samples. The inversion of dual-pol data provides the two biophysical parameters, DBH and tree height. Figure 5 presents the validation results comparing the model-retrieved parameters with ground-truth measurements. The DBH retrieved from the S-band dual-pol data exhibited a relatively weak correlation with the field-measured data, with an R^2 of 0.11, an RMSE of 6.66 cm, and an MAE (%) of 32.63. Similarly, the estimation of tree height showed a lower correlation, with an R^2 of 0.15, an RMSE of 3.19 m, and an MAE (%) of 21.97. For the HH/HV L-band data, the retrieved DBH showed a better correlation with the field-measured data, as indicated by an R^2 of 0.65, an RMSE of 5.16 cm, and an MAE (%) of 26.50. Additionally, the estimation of tree height demonstrated a relatively stronger relationship, with an R^2 of 0.68, an RMSE of 2.12 m, and an MAE (%) of 15.12.
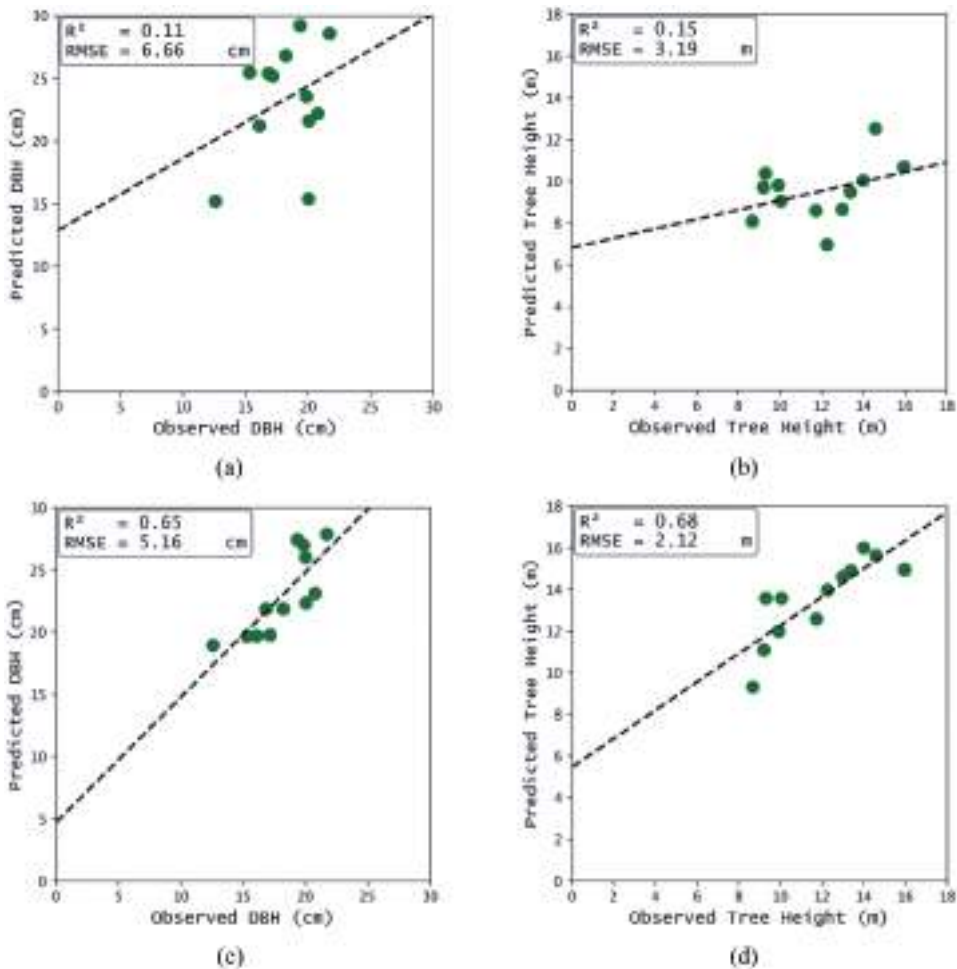

Figure 5. Validation plots for the retrieved DBH and tree height (a & b) from the model inversion of S- band dual-pol data, and validation plots for the retrieved DBH and tree height (c & d) from the model inversion of L- band dual-pol data.

4.1.2. Performance of Model inversion with full-pol data

This section discusses the performance of the model inversion using LS-ASAR full-pol data. In fine-tuning the forward modeling for full-pol data, the vegetation dielectric constant was optimized. This optimal value is held constant during inversion while the free parameters (three in number) are retrieved. The inversion of the full-pol model resulted in the retrieval of DBH, tree height, and tree count per pixel. Figure 6 presents the validation results comparing the model-retrieved parameters with field measurements. The tree count, retrieved using S-band full-pol data, showed a moderate correlation with the field-measured data, evidenced by an R^2 of 0.56, an RMSE of 97.77 trees/ha, and an MAE (%) of 27.59. Further, DBH estimation gave an R^2 of 0.36, an RMSE of 6.23 cm, and an MAE (%) of 32.00. The tree height estimation demonstrated a comparable level of correlation, with an R^2 of 0.34, an RMSE of 2.44 m, and an MAE (%) of 18.60. On the other hand, inverting L-band full-pol data showed much better results. The retrieved tree count exhibited a reasonably strong correlation with field-measured data, with an R^2 of 0.89, an RMSE of 70.90 trees/ha, and an MAE (%) of 26.65. Further, the inversion for DBH estimation displayed a stronger correlation, with an R^2 of 0.74, an RMSE value of 5.00 cm, and an MAE (%) of 25.23. Tree height inversion also demonstrated a stronger correlation with the field values, with an R^2 of 0.71, an RMSE value of 2.10 m, and an MAE (%) of 14.39.

The comparison of the results obtained from the inversion of different biophysical parameters using LS-ASAR data reveals that the L-band full-pol data is most promising in terms of correlation with the field data. It exhibited the strongest correlations and
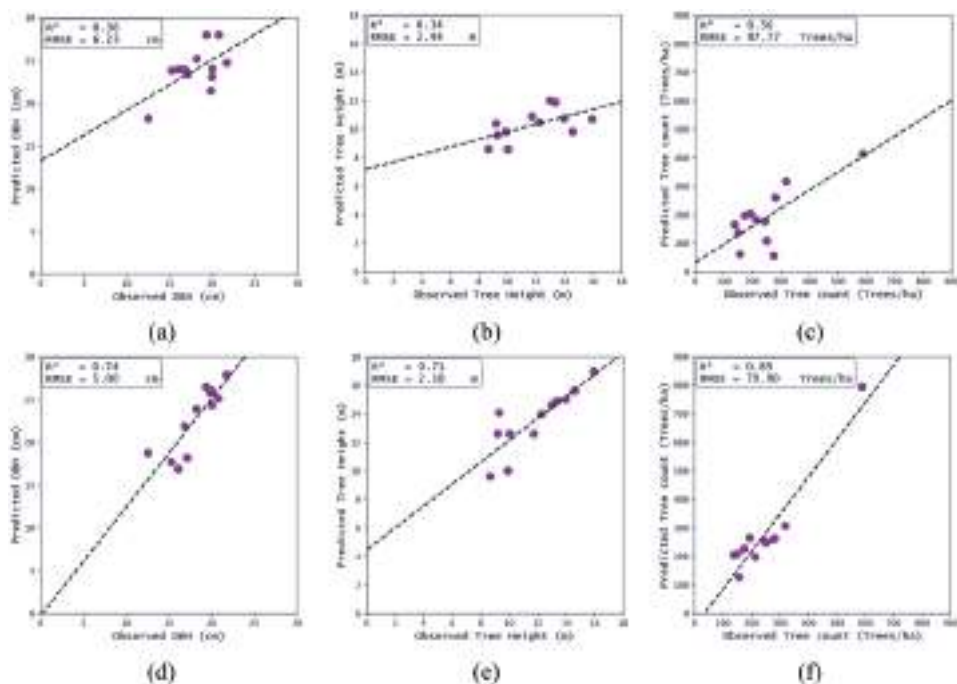

Figure 6. Validation plots for the retrieved DBH (a), tree height (b), and tree count (c) obtained from the model inversion of S- band full polarimetric data, and validation plots for the retrieved DBH (d), tree height (e), and tree count (f) obtained from the model inversion of L- band full polarimetric data.

relatively lower RMSE values for the retrieved tree count, tree height, and DBH. Following the full-pol L-band data, the dual-pol L-band data exhibited favorable results, demonstrating its potential for estimating forest biophysical parameters. Conversely, inverting the S-band full-polarized data revealed average correlations with increased RMSE figures. Meanwhile, inverting the S-band dual-polarized data led to less robust correlations and RMSE values that were notably higher than those in the L-band scenario. Overall, these findings highlight the superiority of the L-band full-polarized data as the most effective approach for retrieving biophysical parameters, followed by L-band dual-pol data. Please note that the P-band case is not evaluated in this study.

4.2. AGB estimation and validation

As mentioned in section 3, for the full-pol case, the model predicted the tree counts for each pixel, along with tree height and DBH. Subsequently, these retrieved tree counts were multiplied with the corresponding AGB values estimated with the allometric equation (see section 2.2), enabling the estimation of the total AGB for each pixel. Accurate retrieval of the tree count plays a critical role in this process, as it provides vital information about the varying tree numbers within each plot and exerts a significant impact on the overall accuracy of the AGB estimation. On the other hand, with dual polarimetric data, the model had no predictive power for the tree count. Instead, a constant optimal value for tree count (as obtained by fine-tuning the forward model) was used in the allometric equation to calculate the total above-ground biomass for the respective plots. This largely explains the statistically significant difference in the accuracy of the estimated AGB between the dual- and full-pol cases.

The geocoded AGB maps prepared for the study area (for both frequencies and for both dual- and full-pol configurations) are shown in Figure 7. These maps illustrate the spatial distribution of predicted above-ground biomass across the selected study area. To ensure accuracy, non-forested areas were masked on the AGB maps, focusing solely on forested regions for the analysis. To expedite the optimization process, resampled SAR images with a pixel size of 30 m × 30 m were utilized. The AGB map employs a color scheme transitioning from yellow to deep blue, indicating increasing AGB values from 0 to > 200 t/ha.

The study area encompassed sites with diverse levels of biomass, and the predicted data reveals a heterogeneous spread of above-ground biomass within the area. The AGB map prepared using L-band full-pol data (Figure 7(d)) showed a significant degree of variability, followed by the dual-pol L-band data (Figure 7(b)). However, compared to the full-pol case, there was a decrease in the extent of variability in the dual-pol case.

In the case of model inversion with the S-band, the majority of pixels were grouped within the lower classes of AGB. This distribution is primarily attributed to the fact that the S-band data has very little sensitivity towards higher biomass ranges. Comparing Figure 7(c,d) shows the significant saturation of the S-band for higher AGB levels (>100 t/ha). This effect is visible even in the dual-pol case (Figure 7(a,b)), confirming that it is indeed a frequency-related effect. Additionally, when using S-band dual polarization, it was observed that the predicted AGB did not surpass the 100–150 t/ha range.

For higher AGB study areas, it may be advantageous to look for L-band dual-pol data over even S-band full-pol data, as will be more evident with the subsequent discussions. It
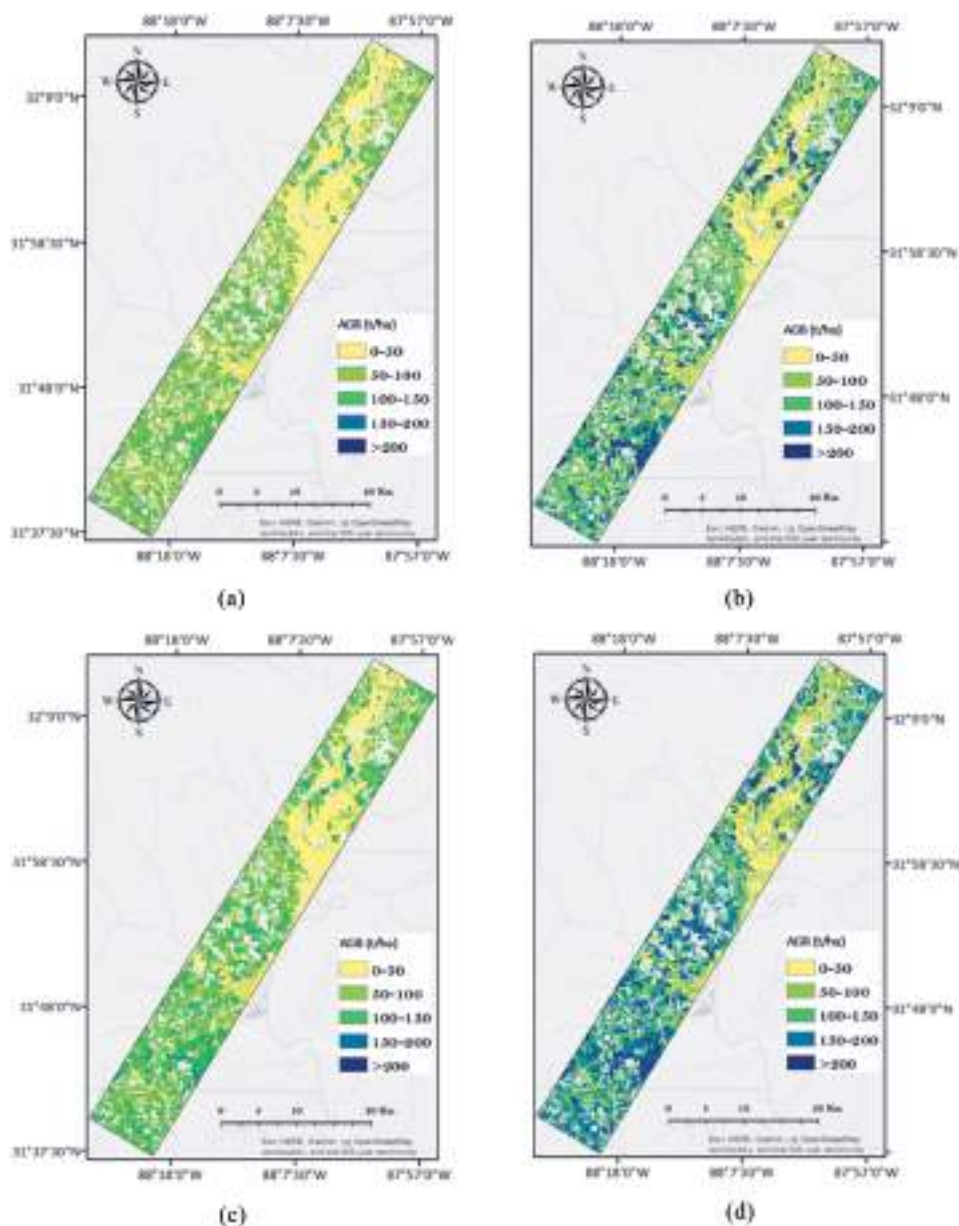
Figure 7. AGB maps from the scattering model for both S- and L- dual polarimetric data (a & b) and S- and L- full polarimetric data (c & d). The regions colored grey in the maps correspond to non-forested areas.

is worth noting that the L-band also reaches saturation at higher AGB values, and the retrieval accuracy goes down drastically. The predictive reliability starts to diminish significantly with L-band data when the biomass exceeds 150 t/ha. Whereas, in the S-band, the accuracy starts to decrease earlier, specifically when the biomass measures go beyond 100 t/ha. It is noticed that, in areas where the biomass is comparatively low, both frequencies provided a relatively high degree of accuracy in predicting AGB.
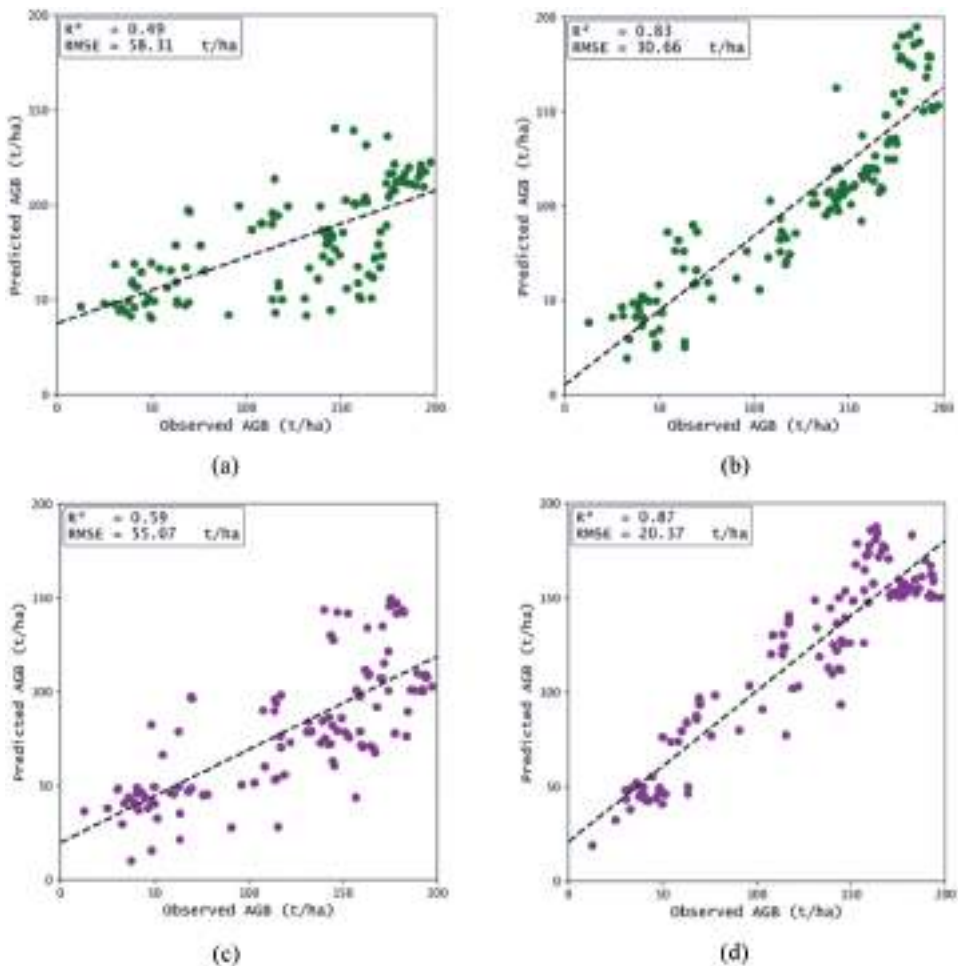
Figure 8. Validation plots for model-predicted AGB against LIDAR-derived and field-measured AGB for S- and L-band dual-pol data (a & b) and S- and L-band full-pol data (c & d).

Figure 8 presents the validation of the AGB maps shown in Figure 7 by comparing the predicted AGB with the LIDAR-derived and field measured AGB (for all the frequency and polarization combinations considered in this paper). These scatter plots display varying performances for different frequencies and different polarization combinations. The estimation of AGB with S-band dual-pol data turned out to have the weakest correlation with the field-measured data, as evidenced by an R^2 of 0.49, an RMSE value of 58.31 t/ha, and an MAE (%) of 39.73. For L-band dual-pol data, the inversion process exhibited a high correlation, with an R^2 of 0.83, an RMSE value of 30.66 t/ha, and an MAE (%) of 21.42, indicating reasonable accuracy in estimating forest AGB which is in fact better than the S-band full-pol case.

When dealing with S-band full-pol data, the results showed a weaker correlation, with an R^2 of 0.59, a higher RMSE value of 55.07 t/ha, and an MAE (%) of 37.45, suggesting that the effectiveness of S-band data for AGB estimation is comparatively limited. Lastly, the inversion of L-band full-pol data demonstrated the strongest performance, indicating

Table 4. Performance evaluation of the scatter model with dual-pol and full-pol ASAR data at L-and S-bands.

Parameter	Evaluation Index	Dual-pol		Full-pol	
		S-band	L-band	S-band	L-band
AGB	R^2	0.49	0.83	0.59	0.87
	RMSE (t/ha)	58.31	30.66	55.07	20.37
	MAE(%)	39.73	21.42	37.45	14.10
Height	R^2	0.15	0.68	0.34	0.71
	RMSE (m)	3.19	2.12	2.44	2.10
	MAE(%)	21.97	15.12	18.60	14.39
DBH	R^2	0.11	0.65	0.36	0.74
	RMSE (cm)	6.66	5.16	6.23	5.00
	MAE(%)	32.63	26.50	32.00	25.23
Tree Count	R^2	-	-	0.56	0.89
	RMSE (No. of trees/ha)	-	-	97.77	70.90
	MAE(%)	-	-	27.59	26.65

a robust correlation and higher accuracy in estimating forest biomass ($R^2 = 0.87$, RMSE = 20.37 t/ha, and MAE (%) = 14.10) for AGB estimation. Overall, these findings highlight the superior performance of the L-band full polarized data in accurately estimating above-ground biomass in temperate forests, followed by the L-band dual polarized data, the S-band full polarized data, and finally the S-band dual polarized data. Table 4 presents an overview of the accuracy assessment.

5. Discussion

The section presents a detailed discussion of the results, comparing them with existing research in the field. This comparison enables clear inferences to be made about the capabilities and limitations of the scattering model when used with the (dual and full-pol) LS-ASAR data in estimating AGB.

Previous investigations (Dobson et al. 1992; Pulliainen, Kurvonen, and Hallikainen 1999; Way et al. 1994) have revealed that the influence of trunk-ground interactions on the overall backscatter at the selected SAR frequencies is expected to be relatively weak. Armed with this knowledge, our approach prioritized the coherent addition of backscatter coefficients from direct ground and trunk interactions to the total backscatter intensity. The utilization of RT models offers distinct advantages over non-parametric models. One notable advantage of RT models is their lower dependency on large reference data sets. While non-parametric models heavily depend on extensive reference data for efficient performance (Hongliang and Shunlin 2003), RT models can operate effectively with a comparatively smaller set of reference data. This study aligns with other research works that have leveraged RT models for AGB estimation with limited reference data. For instance, Wang and Qi (Wang and Qi 2008) successfully employed a first-order RT model to estimate the woody biomass of tropical forests using 32 sampling sites. Similarly, Soja et al. (2021) employed a canopy scatter model with P-band SAR data to estimate AGB with six reference plots. Santoro et al (Santoro et al. 2011). developed a scattering model, which is independent of field data, for the interpretation of ENVISAT ASAR C-band data aimed at mapping the growing stock volume in boreal forests. A similar

technique was also proposed by Cartus et al (Cartus et al. 2011). with ERS-1/2 tandem coherence, which aimed to map different classes of growing stock volume in Northeast China. Compared to empirical models, RT theory-based models exhibit greater reproducibility, as they are less reliant on field data (Houborg, Soegaard, and Boegh 2007; Quan, He, and Li 2015; Yebra et al. 2013). This characteristic enhances the robustness of RT models, making them applicable to a wider range of forested regions and vegetation types.

This study used the allometric relationship introduced by Stovall et al (Stovall et al. 2018). to estimate the above-ground biomass, considering both the trunk DBH and tree height within the designated plots. According to the study conducted by Frank et al (Frank et al. 2018). incorporating tree height into models can aid in accounting for potential differences across various sites. Another study conducted by Lambert et al (Lambert, Ung, and Raulier 2005). demonstrated that incorporating tree height measurement in allometric equations, along with DBH, enables more accurate estimations of tree volume and reduces the root mean squared error of total tree biomass predictions (by approximately 8% for hardwood species and 25% for softwood species).

The results of this study align with the findings of Tanase et al (Tanase et al. 2014), who investigated the impact of employing full pol data versus a dual-polarized system for estimating above-ground biomass using parametric and non-parametric models. In their study, they reported a slight improvement in estimation accuracy (2%) when incorporating all four polarizations. The outcomes of this study are also in line with the results reported by Pereira et al (Pereira et al. 2018), where they investigated the performance of different polarimetric SAR data configurations in univariate and multivariate generalized linear models for AGB estimation. Their study revealed that the most accurate and least biased AGB estimates were obtained using fully polarimetric data from the PALSAR-1 data, which is an L-band system, surpassing the accuracy achieved with single- and dual-pol SAR data. In the present study, the findings are consistent with those presented by Khati et al (Khati et al. 2020), who conducted a comprehensive assessment of forest biomass estimation using L-band SAR backscatter at the Lenoir Landing site. This assessment was carried out using images from the UAVSAR acquired in 2019. In their approach, Khati et al. employed the modified Water Cloud Model (WCM) for biomass estimation, achieving notable accuracy. The results of their study were significant, with an R^2 value of 0.76 and an RMSE of 14.13 t/ha. Similarly, Ghosh et al (Ghosh et al. 2023). carried out a study at the Lenoir Landing site that employed a kernel-based Gaussian process regression (GPR) technique for estimating biomass using data from L-band UAVSAR acquired in 2019. The study achieved notable results, with an R^2 value of 0.73 and an RMSE of 16.50 t/ha. The findings from the current study at the Lenoir Landing site, which employed the RT model in combination with LS-ASAR and LIDAR data, exhibit alignment with the results of previous research conducted in the same region. Uniquely, the present study applies varied polarimetric SAR data configurations to radiative transfer modeling, offering an unexplored comprehensive evaluation approach. This significantly enhances the understanding of biomass estimation accuracy, positioning the current research as a novel contribution to applying diverse SAR configurations for accurate biomass estimation. Table 5 provides a comprehensive comparative overview, juxtaposing relevant AGB estimation studies with the present study.

Table 5. Description of relevant AGB estimation studies.

Ecosystem Type, Study Area	Methodology	Sensor	Biomass Map Scale	Performance matrices (Best)	Field Data	References
Boreal & Temperate forests Northeastern United States	RT model	ALOS PALSAR (L-band, 1.27 GHz)	30 m	R2 = 0.86 RMSE = 12.9 t/ha)	-, 2007	Cartus, Santoro, and Kellndorfer 2012
Temperate forests Vancouver Island, Canada	Empirical regressions	PALSAR (L-band, 1.27 GHz), RADARSAT-2 (C-band, 5.405 GHz), LIDAR	-	R2 = 0.87	18 sites, 2005 & 2008	Tsui et al. 2012
Temperate forests Maine, U.S.A.	Empirical regressions	UAVSAR (L-band, 1.25 GHz)	100 m	R2 = 0.67 RMSE = 44 t/ha	32 sites, 2009 & 2010	Robinson et al. 2013
Temperate forests Marlborough, UK	RT model & Empirical regressions	AirSAR (S-band, 3.1 GHz)	25 m	R2 = 0.47 RMSE = 97.91 t/ha	78 sites, 2012 & 2015	Ningthoujam et al. 2016
Temperate forests Lenoir Landing site, U.S.A.	RT model	UAVSAR (L-band, 1.25 GHz) & LIDAR	-	R2 = 0.76 RMSE = 14.13 t/ha	51 sites, 2019	Khati et al. 2020
Temperate forests California, U.S.A.	Parametric models	GEDI, ICESat-2, UAVSAR (L-band, 1.25 GHz) & Airborne laser scanning	30m	R2 = 0.63 RMSE = 110.95 t/ha	-, -	Silva et al. 2021
Coniferous Forest Mongolia, China	Non-parametric model	ALOS-2 PALSAR-2 (L-band, 1.5 GHz) GF-3 (L-band, 5.4 GHz)	30 m	R2 = 0.93 RMSE = 10.42 t/ha	50 sites, 2021 & 2010	Hu et al. 2023
Temperate forests Lenoir Landing site, U.S.A.	Non-parametric model	UAVSAR (L-band, 1.25 GHz) & LIDAR	20m, 30m, 50m & 100m	R2 = 0.73 RMSE = 16.50 t/ha	-, 2019	Ghosh et al. 2023
Temperate forests Lenoir Landing site, U.S.A.	**RT model**	**LS-ASAR (L-band, 1.25 GHz) & LIDAR**	**30m**	**R2 = 0.87 RMSE = 20.37 t/ha**	**14 sites, 2021**	**Present study**
Temperate forests Lenoir Landing site, U.S.A.	**RT model**	**LS-ASAR (S-band, 3.2 GHz) & LIDAR**	**30m**	**R2 = 0.59 RMSE = 55.07 t/ha**	**14 sites, 2021**	**Present study**

6. Conclusion

The present study explored the use of LS-ASAR backscatter in dual polarization and full polarization modes for the estimation of AGB in the study area (the temperate forests of the Lenoir landing site in Southwest Alabama, United States of America). In a vegetation stand, the predominant share of the AGB resides within the woody components. This understanding influenced our decision to adopt a cylinder scattering model, where the canopy is conceptualized as a layer of defoliated trunks and illustrated as an assortment of dielectric cylinders distributed randomly and possessing fixed heights. For the retrieval of forest biophysical parameters, the study integrated the dielectric cylinder scatter model with the I^2EM surface scatter model. This integrated scattering model was inverted either with the full polarization data (HH/HV/VV) or with the dual polarization data (HH/HV). A small portion of the ground truth data was utilized to fine-tune the parameters of the forward model, with the rest serving as independent validation data. RT models stand out for their robustness and wide applicability, as they have less dependence on reference data. The study utilized an allometric equation to estimate AGB, which incorporated height, DBH, and tree count. The use of full-pol data allowed the estimation of tree counts for each pixel in addition to DBH and tree height, facilitating more accurate AGB estimation. The results of AGB estimation revealed varying performances for different combinations of frequency and polarization. The strongest performance in AGB estimation was noted in the inversion of L-band fully polarized data, with a high correlation ($R^2 = 0.87$) and the lowest RMSE (20.37 t/ha). The inversion of L-band dual polarized data, S-band fully polarized data, and S-band dual polarized data, in that order, showed progressively lower correlations and higher RMSE values.

The use of LS-ASAR backscatter data in dual and full polarization, integrated with radiative transfer models, presents a viable approach for estimating AGB in temperate forest ecosystems. Among the methods studied, the retrieval process exhibited superior performance with the L-band full polarized data inversion, making it the most effective approach for retrieving biophysical parameters in the study area. However, the presence of non-negligible RMSE values implies that there is room for further refinement in the model to achieve more accurate AGB estimates. The factors contributing to the observed discrepancies between the retrieved and measured parameters include variations in forest structure, species compositions, terrain characteristics, and data acquisition conditions. Future research may seek to extend these findings by optimizing the inversion process and investigating the potential of the fusion of different modalities and polarizations. The findings from this research offer important direction for future investigations and advancements in the field of SAR-based above-ground biomass estimation techniques.

Disclosure statement

No potential conflict of interest was reported by the authors.

ORCID

Faseela V. Sainuddin http://orcid.org/0000-0002-2686-3563
Sanid Chirakkal http://orcid.org/0000-0001-7439-5154
Smitha V. Asok http://orcid.org/0000-0002-7393-2584
Deepak Putrevu http://orcid.org/0000-0002-3866-7025

Data Availability statement

The LS-ASAR products are freely available at https://uavsar.jpl.nasa.gov/cgi-bin/asar.py.

References

Antropov, O., Y. Rauste, H. Ahola, and T. Hame. 2013. "Stand-Level Stem Volume of Boreal Forests from Spaceborne SAR Imagery at L-Band." *IEEE Journal of Selected Topics in Applied Earth Observations and Remote Sensing* 6 (1): 35–44. https://doi.org/10.1109/JSTARS.2013.2241018.

Askne, J. I. H., M. Santoro, G. Smith, and J. E. S. Fransson. 2003. "Multitemporal Repeat-Pass SAR Interferometry of Boreal Forests." *IEEE Transactions on Geoscience and Remote Sensing* 41 (7): 1540–1550. https://doi.org/10.1109/TGRS.2003.813397.

Baker, J., and A. Luckman. 1999. "Microwave Observations of Boreal Forests in the NOPEX Area of Sweden and a Comparison with Observations of a Temperate Plantation in the United Kingdom." *Agricultural and Forest Meteorology* 98–99:389–416. https://doi.org/10.1016/S0168-1923(99)00111-2.

Balzter, H., J. Baker, M. T. Hallikainen, and E. Tomppo. 2002. "Retrieval of Timber Volume and Snow Water Equivalent Over a Finnish Boreal Forest from Airborne Polarimetric Synthetic Aperture Radar." *International Journal of Remote Sensing* 23 (16): 3185–3208. https://doi.org/10.1080/01431160110076199.

Bouvet, A., S. Mermoz, T. Le Toan, L. Villard, R. Mathieu, L. Naidoo, and G. P. Asner. 2018. "An Above-Ground Biomass Map of African Savannahs and Woodlands at 25 M Resolution Derived from ALOS PALSAR." *Remote Sensing of Environment* 206:156–173. https://doi.org/10.1016/j.rse.2017.12.030.

Breidenbach, J., E. Næsset, and T. Gobakken. 2012. "Improving K-Nearest Neighbor Predictions in Forest Inventories by Combining High and Low Density Airborne Laser Scanning Data." *Remote Sensing of Environment* 117:358–365. https://doi.org/10.1016/j.rse.2011.10.010.

Bryant, R., M. S. Moran, D. P. Thoma, C. H. Collins, S. Skirvin, M. Rahman, K. Slocum, P. Starks, D. Bosch, and M. G. Dugo. 2007. "Measuring Surface Roughness Height to Parameterize Radar Backscatter Models for Retrieval of Surface Soil Moisture." *IEEE Geoscience and Remote Sensing Letters* 4 (1): 137–141. https://doi.org/10.1109/LGRS.2006.887146.

Cartus, O., M. Santoro, and J. Kellndorfer. 2012. "Mapping Forest Aboveground Biomass in the Northeastern United States with ALOS PALSAR Dual-Polarization L-Band." *Remote Sensing of Environment* 124:466–478. https://doi.org/10.1016/j.rse.2012.05.029.

Cartus, O., M. Santoro, C. C. Schmullius, and Z. Li. 2011. "Large Area Forest Stem Volume Mapping in the Boreal Zone Using Synergy of ERS-1/2 Tandem Coherence and MODIS Vegetation Continuous Fields." *Remote Sensing of Environment* 115:931–943. https://doi.org/10.1016/j.rse.2010.12.003.

Castel, T., A. Beaudoin, N. Stach, N. Stussi, T. Le Toan, and P. Durand. 2001. "Sensitivity of Space-Borne SAR Data to Forest Parameters Over Sloping Terrain Theory and Experiment." *International Journal of Remote Sensing* 22 (12): 2351–2376. https://doi.org/10.1080/01431160121407.

Castro, K. L., G. A. Sanchez-Azofeifa, and B. Rivard. 2003. "Monitoring Secondary Tropical Forests Using Space-Borne Data: Implications for Central America." *International Journal of Remote Sensing* 24 (9): 1853–1894. https://doi.org/10.1080/01431160210154056.

Chauhan, N. S., R. Lang, and K. J. Ranson. 1991. "Radar Modeling of a Boreal Forest." *IEEE Transactions on Geoscience and Remote Sensing* 29 (4): 627–638. https://doi.org/10.1109/36.135825.

Dobson, M. C., F. T. Ulaby, T. LeToan, A. Beaudoin, E. S. Kasischke, and N. Christensen. 1992. "Dependence of Radar Backscatter on Coniferous Forest Biomass." *IEEE Transactions on Geoscience and Remote Sensing* 30 (2): 412–415. https://doi.org/10.1109/36.134090.

Dobson, M. C., F. T. Ulaby, L. E. Pierce, T. L. Sharick, K. M. Bergen, J. Kellndorfer, J. R. Kendra, et al. 1995. "Estimation of Forest Biophysical Characteristics in Northern Michigan with SIRC/X-SAR." *IEEE Transactions on Geoscience & Remote Sensing* 33 (4): 877–895. https://doi.org/10.1109/36.406674.

Dubois, P. C., J. Van Zyl, and T. Engman. 1995. "Measuring Soil Moisture with Imaging Radars." *IEEE Transactions on Geoscience and Remote Sensing* 33 (4): 915–926. https://doi.org/10.1109/36.406677.

Du, Y., F. T. Ulaby, and M. C. Dobson. 2000. "Sensitivity to Soil Moisture by Active and Passive Microwave Sensors." *IEEE Transactions on Geoscience and Remote Sensing* 38 (1): 105–114. https://doi.org/10.1109/36.823905.

European Space Agency. 2008. *Candidate Earth Explorer Core Missions – Reports for Assessment: BIOMASS. ESA SP-1313/2 (6 Volume Series)*. Noordwijk, The Netherlands: European Space Agency.

Frank, J., M. Castle, J. A. Westfall, A. R. Weiskittel, D. W. MacFarlane, S. Baral, P. J. Radtke, and G. Pelletier. 2018. "Variation in Occurrence and Extent of Internal Stem Decay in Standing Trees Across the Eastern US and Canada: Evaluation of Alternative Modelling Approaches and Influential Factors." *Forestry: An International Journal of Forest Research* 91 (3): 382–399. https://doi.org/10.1093/forestry/cpx054.

Fung, A. K., and K. S. Chen. 2010. *Microwave Scattering and Emission Models for Users*. first ed. Norwood, MA, USA: Artech House.

Ghosh, S. S., U. Khati, S. Kumar, A. Bhattacharya, and M. Lavalle. 2023. "Gaussian Process Regression-Based Forest Above Ground Biomass Retrieval from Simulated L-Band NISAR Data." *International Journal of Applied Earth Observation and Geoinformation* 118:103252. https://doi.org/10.1016/j.jag.2023.103252.

Goldberg, D. 1989. *Genetic Algorithms in Search, Optimization, and Machine Learning*. Boston, MA, USA: Addison-Wesley Longman Publishing Co., Inc.

Harrell, P. A., E. S. Kasischke, L. L. Bourgeau-Chavez, E. M. Haney, and N. L. Christensen Jr. 1997. "Evaluation of Approaches to Estimating Aboveground Biomass in Southern Pine Forests Using SIR-C Data." *Remote Sensing of Environment* 59:223–233. https://doi.org/10.1016/S0034-4257(96)00155-1.

Hoekman, D. H., and M. J. Quiriones. 2000. "Land Cover Type and Biomass Classification Using AirSAR Data for Evaluation of Monitoring Scenarios in the Colombian Amazon." *IEEE Transactions on Geoscience and Remote Sensing* 38 (2): 685–696. https://doi.org/10.1109/36.841998.

Hongliang, F., and L. Shunlin. 2003. "Retrieving Leaf Area Index with a Neural Network Method: Simulation and Validation." *IEEE Transactions on Geoscience and Remote Sensing* 41 (9): 2052–2062. https://doi.org/10.1109/TGRS.2003.813493.

Houborg, R., H. Soegaard, and E. Boegh. 2007. "Combining Vegetation Index and Model Inversion Methods for the Extraction of Key Vegetation Biophysical Parameters Using Terra and Aqua MODIS Reflectance Data." *Remote Sensing of Environment* 106 (1): 39–58. https://doi.org/10.1016/j.rse.2006.07.016.

Hu, Y., Y. Nie, Z. Liu, G. Wu, and W. Fan. 2023. "Improving the Potential of Coniferous Forest Aboveground Biomass Estimation by Integrating C-And L-Band SAR Data with Feature Selection and Non-Parametric Model." *Remote Sensing* 15 (17): 4194. https://doi.org/10.3390/rs15174194.

Imhoff, M. L. 1995. "Radar Backscatter and Biomass Saturation: Ramification for Global Biomass Inventory." *IEEE Transactions on Geoscience and Remote Sensing* 33 (2): 511–518. https://doi.org/10.1109/TGRS.1995.8746034.

JPL. 2022. UAVSAR. Accessed December 19, 2022. https://uavsar.jpl.nasa.gov/cgi-bin/asar.py.

Jung, J., S. Kim, S. Hong, K. Kim, E. Kim, J. Im, and J. Heo. 2013. "Effects of National Forest Inventory Plot Location Error on Forest Carbon Stock Estimation Using K-Nearest Neighbor Algorithm." *Isprs Journal of Photogrammetry & Remote Sensing* 81:82–92. https://doi.org/10.1016/j.isprsjprs.2013.04.008.

Karam, M. A., F. Amar, A. K. Fung, E. Mougin, A. Lopes, D. M. Le Vine, and A. Beaudoin. 1995. "A Microwave Polarimetric Scattering Model for Forest Canopies Based on Vector Radiative Transfer Theory." *Remote Sensing of Environment* 53 (1): 16–30. https://doi.org/10.1016/0034-4257(95)00048-6.

Karam, M. A., and A. K. Fung. 1982. "Vector Forward Scattering Theorem." *Radio Science* 17 (4): 752–756. https://doi.org/10.1029/RS017i004p00752.

Karam, M. A., and A. K. Fung. 1988. "Electromagnetic Scattering from a Layer of Finite Length, Randomly Oriented, Dielectric, Circular Cylinders Over a Rough Interface with Application to Vegetation." *International Journal of Remote Sensing* 9 (6): 1109–1134. https://doi.org/10.1080/01431168808954918.

Khati, U., M. Lavalle, G. H. Shiroma, V. Meyer, and B. Chapman. 2020. "Assessment of Forest Biomass Estimation from Dry and Wet SAR Acquisitions Collected During the 2019 UAVSAR AM-PM Campaign in Southeastern United States." *Remote Sensing* 12 (20): 3397. https://doi.org/10.3390/rs12203397.

Kurvonen, L., J. Pulliainen, and M. Hallikainen. 1999. "Retrieval of Biomass in Boreal Forests from Multitemporal ERS-1 and JERS-1 SAR Images." *IEEE Transactions on Geoscience and Remote Sensing* 37 (1): 198–205. https://doi.org/10.1109/36.739154.

Lambert, M. C., C. H. Ung, and F. Raulier. 2005. "Canadian National Tree Aboveground Biomass Models." *Canadian Journal of Forest Research* 35 (8): 1996–2018. https://doi.org/10.1139/x05-112.

Le Toan, T., S. Quegan, M. Davidson, H. Balzter, P. Paillou, K. Papathanassiou, S. Plummer, et al. 2011. "The BIOMASS Mission: Mapping Global Forest Biomass to Better Understand the Terrestrial Carbon Cycle." *Remote Sensing of Environment* 115 (11): 2850–2860. https://doi.org/10.1016/j.rse.2011.03.020.

Lucas, R., J. Armston, R. Fairfax, R. Fensham, A. Accad, J. Carreiras, J. Kelley, P. Bunting, D. Clewley, and S. Bray. 2010. "An Evaluation of the ALOS Palsar L-Band Backscatter—Above Ground Biomass Relationship Queensland, Australia: Impacts of Surface Moisture Condition and Vegetation Structure." *IEEE Journal of Selected Topics in Applied Earth Observations & Remote Sensing* 3 (4): 576–593. https://doi.org/10.1109/JSTARS.2010.2086436.

Luckman, A., J. Baker, and U. Wegmueller. 2000. "Repeat-Pass Interferometric Coherence Measurements of Disturbed Tropical Forest from JERS and ERS Satellites." *Remote Sensing of Environment* 73 (3): 350–360. https://doi.org/10.1016/S0034-4257(00)00110-3.

Martin, A. R., S. C. Thomas, and J. Chave. 2011. "A Reassessment of Carbon Content in Tropical Trees." *PloS ONE* 6 (8): e23533. https://doi.org/10.1371/journal.pone.0023533.

McRoberts, R. E., T. Gobakken, and E. Næsset. 2012. "Post-Stratified Estimation of Forest Area and Growing Stock Volume Using Lidar-Based Stratifications." *Remote Sensing of Environment* 125:157–166. https://doi.org/10.1016/j.rse.2012.07.002.

Mitchard, E. T. A., T. R. Feldpausch, R. J. W. Brienen, G. Lopez-Gonzalez, A. Monteagudo, T. R. Baker, and S. L. Lewis. 2014. "Markedly Divergent Estimates of Amazon Forest Carbon Density from Ground Plots and Satellites." *Global Ecology and Biogeography* 23 (8): 935–946. https://doi.org/10.1111/geb.12168.

Mitchard, E., S. Saatchi, A. Baccini, G. Asner, S. Goetz, N. Harris, and S. Brown. 2013. "Uncertainty in the Spatial Distribution of Tropical Forest Biomass: A Comparison of Pan-Tropical Maps." *Carbon Balance and Management* 7–8 (1): 1–13. https://doi.org/10.1186/1750-0680-8-10.

Modava, M., G. Akbarizadeh, and M. Soroosh. 2018. "Integration of Spectral Histogram and Level Set for Coastline Detection in SAR Images." *IEEE Transactions on Aerospace and Electronic Systems* 55 (2): 810–819. https://doi.org/10.1109/TAES.2018.2865120.

Modava, M., G. Akbarizadeh, and M. Soroosh. 2019. "Hierarchical Coastline Detection in SAR Images Based on Spectral–Textural Features and Global–Local Information." *IET Radar, Sonar & Navigation* 13 (12): 2183–2195. https://doi.org/10.1049/iet-rsn.2019.0063.

Morales, J. L. 2002. "Numerical Study of Limited Memory BFGS Methods." *Applied Mathematics Letters* 15 (4): 481–487. https://doi.org/10.1016/S0893-9659(01)00162-8.

MRLC. 2022. "National Landcover Database." Accessed January 19, 2023. https://www.mrlc.gov/.

Mutanga, O., E. Adam, and M. A. Cho. 2012. "High Density Biomass Estimation for Wetland Vegetation Using worldView-2 Imagery and Random Forest Regression Algorithm." *International Journal of Applied Earth Observation and Geoinformation* 18:399–406. https://doi.org/10.1016/j.jag.2012.03.012.

Naidoo, L., R. Mathieu, R. Main, W. Kleynhans, K. Wessels, G. Asner, and B. Leblon. 2015. "Savannah Woody Structure Modelling and Mapping Using Multi-Frequency (X-, C- and L-Band) Synthetic Aperture Radar Data." *Isprs Journal of Photogrammetry & Remote Sensing* 105:234–250. https://doi.org/10.1016/j.isprsjprs.2015.04.007.

NEON. 2020. "Lenoir landing NEON/LENO." Accessed December 20, 2022. https://www.neonscience.org/field-sites/leno .

Neumann, M., S. Saatchi, L. M. H. Ulander, and J. E. S. Fransson. 2012. "Assessing Performance of L- and P-Band Polarimetric Interferometric SAR Data in Estimating Boreal Forest Above-Ground Biomass." *IEEE Transactions on Geoscience and Remote Sensing* 50 (3): 714–726. https://doi.org/10.1109/TGRS.2011.2176133.

Ningthoujam, R. K., H. Balzter, K. Tansey, T. R. Feldpausch, E. T. Mitchard, A. Wani, and P. K. Joshi. 2017. "Relationships of S-Band Radar Backscatter and Forest Aboveground Biomass in Different Forest Type." *Remote Sensing* 9 (11): 1116. https://doi.org/10.3390/rs9111116.

Ningthoujam, R. K., H. Balzter, K. Tansey, K. Morrison, S. C. M. Johnson, F. Gerard, C. George, et al. 2016. "Airborne S-Band SAR for Forest Biophysical Retrieval in Temperate Mixed Forests of the UK." *Remote Sensing* 8:609. https://doi.org/10.3390/rs8070609.

NISAR. 2020. "NASA-ISRO SAR Mission (NISAR)." Accessed December 20, 2022. https://nisar.jpl.nasa.gov/.

Oh, Y., K. Sarabandi, and F. T. Ulaby. 1992. "An empirical model and an inversion technique for radar scattering from bare soil surfaces." *IEEE Transactions on Geoscience and Remote Sensing* 30 (2): 370–381. https://doi.org/10.1109/36.134086.

Pereira, L. O., L. F. A. Furtado, E. M. L. M. Novo, S. J. S. Sant'anna, V. Liesenberg, and T. S. F. Silva. 2018. "Multifrequency and Full-Polarimetric SAR Assessment for Estimating Above Ground Biomass and Leaf Area Index in the Amazon Várzea Wetlands." *Remote Sensing* 10:1355. https://doi.org/10.3390/rs10091355.

Periasamy, S. 2018. "Significance of dual polarimetric synthetic aperture radar in biomass retrieval: An attempt on Sentinel-1." *Remote Sensing of Environment* 217:537–549. https://doi.org/10.1016/j.rse.2018.09.003.

Pulliainen, J. T., L. Kurvonen, and M. T. Hallikainen. 1999. "Multitemporal Behavior of L- and C-Band SAR Observations of Boreal Forests." *IEEE Transactions on Geoscience and Remote Sensing* 37 (2): 927–937. https://doi.org/10.1109/36.752211.

Quan, X. W., B. B. He, and X. Li. 2015. "A Bayesian Network-Based Method to Alleviate the Ill-Posed Inverse Problem: A Case Study on Leaf Area Index and Canopy Water Content Retrieval." *Remote Sensing of Environment* 53 (12): 6507–6517. https://doi.org/10.1109/TGRS.2015.2442999.

Quegan, S., T. Le Toan, J. Dall, J. F. Exbrayat, D. H. T. Minh, M. M. d'Alessandro, P. Paillou, et al. 2019. "The European Space Agency BIOMASS Mission: Measuring Forest Above-Ground Biomass from Space." *Remote Sensing of Environment* 227:44–60. https://doi.org/10.1016/j.rse.2019.03.032.

Ranson, K. J., and G. Sun. 1994. "Mapping Biomass of a Northern Forest Using Multifrequency SAR Data." *IEEE Transactions on Geoscience and Remote Sensing* 32 (2): 388–396. https://doi.org/10.1109/36.295053.

Robinson, C., S. Saatchi, M. Neumann, and T. Gillespie. 2013. "Impacts of Spatial Variability on Aboveground Biomass Estimation from L-Band Radar in a Temperate Forest." *Remote Sensing* 5 (3): 1001–1023. https://doi.org/10.3390/rs5031001.

Saatchi, S., N. Harris, S. Brown, M. Lefsky, E. T. Mitchard, W. Salas, B. R. Zutta, et al. 2011. "Benchmark Map of Forest Carbon Stocks in Tropical Regions Across Three Continents." *Proceedings of the National Academy of Sciences of the United States of America* 108 (24): 9899–9904. https://doi.org/10.1073/pnas.1019576108.

Saatchi, S., R. A. Houghton, R. C. Alvala, J. V. Soares, and Y. YU. 2007. "Distribution of Above-Ground Live Biomass in the Amazon Basin." *Global Change Biology* 13 (4): 816–837. https://doi.org/10.1111/j.1365-2486.2007.01323.x.

Saatchi, S., Y. Malhi, B. Zutta, W. Buermann, L. O. Anderson, A. M. Araujo, O. L. Phillips, et al. 2009. "Mapping landscape scale variations of forest structure, biomass, and productivity in Amazonia." *Biogeosciences Discussions* 6:5461–5505. https://doi.org/10.5194/bgd-6-5461-2009.

Saatchi, S., and K. C. McDonald. 1997. "Coherent Effects in Microwave Backscattering Models for Forest Canopies." *IEEE Transactions on Geoscience and Remote Sensing* 35 (4): 1032–1044. https://doi.org/10.1109/36.602545.

Sainuddin, F. V., S. Chirakkal, V. S. Asok, K. A. Das, and D. Putrevu. 2023. "Evaluation of Multifrequency SAR Data for Estimating Tropical Above-Ground Biomass by Employing Radiative Transfer Modeling." *Environmental Monitoring and Assessment* 195 (9): 1102. https://doi.org/10.1007/s10661-023-11715-7.

Sainuddin, F. V., S. Chirakkal, V. S. Asok, and D. Putrevu. 2021. "Forest Stand Height Estimation by Inversion of Polarimetric Canopy Scattering Models." In *IEEE International India Geoscience and Remote Sensing Symposium (InGARSS)* 532–536. https://doi.org/10.1109/InGARSS51564.2021.9791867.

Sandberg, G., L. M. H. Ulander, J. E. S. Fransson, J. Holmgren, and T. Le Toan. 2011. "L- and P-Band Backscatter Intensity for Biomass Retrieval in Hemiboreal Forest." *Remote Sensing of Environment* 115:2874–2886. https://doi.org/10.1016/j.rse.2010.03.018.

Santoro, M., C. Beer, O. Cartus, C. C. Schmullius, A. Shvidenko, I. McCallum, U. Wegmüller, and A. Wiesmann. 2011. "Retrieval of Growing Stock Volume in Boreal Forest Using Hyper-Temporal Series of Envisat ASAR ScanSAR Backscatter Measurements." *Remote Sensing of Environment* 115 (2): 490–507. https://doi.org/10.1016/j.rse.2010.09.018.

Santoro, M., and O. Cartus. 2018. "Research Pathways of Forest Above-Ground Biomass Estimation Based on SAR Backscatter and Interferometric SAR Observations." *Remote Sensing* 10 (4): 608–631. https://doi.org/10.3390/rs10040608.

Santoro, M., L. E. B. Eriksson, J. I. H. Askne, and C. C. Schmullius. 2006. "Assessment of Stand-Wise Stem Volume Retrieval in Boreal Forest from JERS-1 L-Band SAR Backscatter." *International Journal of Remote Sensing* 27 (16): 3425–3453. https://doi.org/10.1080/01431160600646037.

Santoro, M., J. E. S. Fransson, L. E. B. Eriksson, M. Magnusson, L. M. H. Ulander, and H. Olsson. 2009. "Signatures of ALOS PALSAR L-Band Backscatter in Swedish Forest." *IEEE Transactions on Geoscience and Remote Sensing* 47 (12): 4001–4019. https://doi.org/10.1109/TGRS.2009.2023906.

Santos, J. R., C. C. Freitas, L. S. Araujo, L. V. Dutra, J. C. Mura, F. F. Gama, L. S. Soler, and S. J. S. SantAnna. 2003. "Airborne P-Band SAR Applied to the Aboveground Biomass Studies in the Brazilian Tropical Rainforest." *Remote Sensing of Environment* 87 (4): 482–493. https://doi.org/10.1016/j.rse.2002.12.001.

Shi, J., J. Wang, A. Y. Hsu, P. E. O'Neill, and E. T. Engman. 1997. "Estimation of Bare Surface Soil Moisture and Surface Roughness Parameter Using L-Band SAR Image Data." *IEEE Transactions on Geoscience and Remote Sensing* 35 (5): 1254–1266. https://doi.org/10.1109/36.628792.

Silva, C. A., L. Duncanson, S. Hancock, A. Neuenschwander, N. Thomas, M. Hofton, M. Fatoyinbo, et al. 2021. "Fusing Simulated GEDI, ICESat-2 and NISAR Data for Regional Aboveground Biomass Mapping." *Remote Sensing of Environment* 253:112234. https://doi.org/10.1016/j.rse.2020.112234.

Skriver, H., H. B. Mortensen, and P. Gudmandsen. 1994. "Calibration and Modelling of MAESTRO 1 Polarimetric SAR Data of a Forest Area in Les Landes, France." *International Journal of Remote Sensing* 15 (14): 2737–2754. https://doi.org/10.1080/01431169408954282.

Soja, M. J., S. Quegan, M. M. D. Alessandro, F. Banda, K. Scipal, S. Tebaldini, and L. M. H. Ulander. 2021. "Mapping Above-Ground Biomass in Tropical Forests with Ground-Cancelled P-Band SAR and Limited Reference Data." *Remote Sensing of Environment* 253:1153–1169. https://doi.org/10.1016/j.rse.2020.112153.

Stovall, A. E. L., H. H. Shugart, A. E. L. Stovall, and K. J. Anderson-Teixeira. 2018. "Assessing Terrestrial Laser Scanning for Developing Nondestructive Biomass Allometry." *Forest Ecology and Management* 427:217–229. https://doi.org/10.1016/j.foreco.2018.06.004.

Tanase, M. A., R. Panciera, K. Lowell, S. Tian, J. M. Hacker, and J. P. Walker. 2014. "Airborne multi-temporal L-band polarimetric SAR data for biomass estimation in semi-arid forests." *Remote Sensing of Environment* 145:93–104. https://doi.org/10.1016/j.rse.2014.01.024.

Topp, G. C., J. L. Davis, and A. P. Annan. 1980. "Electromagnetic determination of soil water content: Measurements in coaxial transmission lines." *Water Resources Research* 16 (3): 574–582. https://doi.org/10.1029/WR016i003p00574.

Tsui, O. W., N. C. Coops, M. A. Wulder, P. L. Marshall, and A. McCardle. 2012. "Using Multi-Frequency Radar and Discrete-Return LiDar Measurements to Estimate Above-Ground Biomass and Biomass Components in a Coastal Temperate Forest." *ISPRS Journal of Photogrammetry and Remote Sensing* 69:121–133. https://doi.org/10.1016/j.isprsjprs.2012.02.009.

Van der Werf, G. R., D. C. Morton, R. S. DeFries, J. G. J. Olivier, P. S. Kasibhatla, R. B. Jackson, G. J. Collatz, and J. T. Randerson. 2009. "CO2 emissions from forest loss." *Nature Geoscience* 2:737–738. https://doi.org/10.1038/ngeo671.

Wait, J. R. 1955. "Scattering Plane Wave from a Circular Dielectric Cylinder at Oblique Incidence." *Canadian Journal of Physics* 33 (5): 189–195. https://doi.org/10.1139/p55-024.

Wait, J. R. 1959. *Electromagnetic Radiation from Cylindrical Structure*. New York, USA: Pergamon Press.

Wang, C., and J. Qi. 2008. "Biophysical Estimation in Tropical Forests Using JERS-1 SAR and VNIR Imagery. II. Aboveground Woody Biomass." *International Journal of Remote Sensing* 29 (23): 6827–6849. https://doi.org/10.1080/01431160802270123.

Way, J., E. Rignot, K. C. McDonald, R. Oren, R. Kwok, G. Bonan, M. C. Dobson, L. A. Viereck, and J. E. Roth. 1994. "Evaluating the Type and State of Alaska Taiga Forests with Imaging Radar for Use in Ecosystem Models." *IEEE Transactions on Geoscience & Remote Sensing* 32 (2): 353–370. https://doi.org/10.1109/36.295050.

Yebra, M., P. E. Dennison, E. Chuvieco, D. Riano, P. Zylstra, P. Hunt, E. R. Danson, F. M. Qi, and S. Jurdao. 2013. "A Global Review of Remote Sensing of Live Fuel Moisture Content for Fire Danger Assessment: Moving Towards Operational Products." *Remote Sensing of Environment* 136:455–468. https://doi.org/10.1016/j.rse.2013.05.029.